Decay of symmetry-protected quantum states

Anna A. Bychek,[1] Dmitrii N. Maksimov,[1,2] and Andrey R. Kolovsky[1,2]
[1]*LV Kirensky Institute of Physics, Federal Research Center KSC SB RAS, 660036 Krasnoyarsk, Russia*
[2]*Siberian Federal University, 660041 Krasnoyarsk, Russia*

(Received 17 June 2020; accepted 25 August 2020; published 15 September 2020)

We study the decay of bosonic many-body states in the triple-well Bose-Hubbard model where bosons in the central well can escape into a reservoir. For vanishing interparticle interaction this system supports a nondecaying many-body state which is the antisymmetric Bose-Einstein condensate with particles occupying only the edge wells. In the classical approach this quantum state corresponds to a symmetry-protected nondecaying state which is stable even at finite interaction below a certain intensity threshold. Here we demonstrate that despite the fact that the classical counterpart is stable the antisymmetric Bose-Einstein condensate is always metastable at finite interatomic interactions due to quantum fluctuations.

DOI: 10.1103/PhysRevA.102.033324

I. INTRODUCTION

Dissipative quantum systems are of great importance as they pave a way for manipulating quantum matter for preparation of pure [1] as well as highly entangled [2] states, and implementation of quantum computations [3]. One particular example of dissipative quantum systems realized with cold atoms are open systems which can exchange particles with a reservoir [4–10], so, neither the energy nor the particle number is preserved. If an open system is coupled with two reservoirs with different chemical potentials, it realizes an atomtronic analog [11] of semiconductor devices [7,9,10,12,13]. Alternatively a quantum lattice system can be coupled with the environment only in a single lattice site as experimentally demonstrated in [14].

Here we consider decay of Bose particles from a triple quantum well with the central well coupled to the environment, i.e., the bosonic particles are drained into a reservoir [15]. Despite its simplicity the three-site Bose-Hubbard (BH) model does not allow for the exact analytic solution [15–19]. In this paper we employ the pseudoclassical approach [20–28] which allows us to cast the problem into a form of coupled driven nonlinear oscillators. From the pure classical perspective this system supports a nondecaying solution with equal intensities but opposite phases on the edge sites. Such a solution has a zero amplitude at the central site, and, therefore, is not directly coupled to the reservoir. This kind of localized solution, existing in the system despite the fact that loss channels are allowed, is known as a bound state in the continuum (BIC) [29]. In particular, the BIC to be considered in the present work is analogous to that supported by a pair of side defects coupled to photonic crystalline waveguides [30,31]. From the quantum mechanical perspective the discussed BIC is the antisymmetric Bose-Einstein condensate (BEC) with particles occupying only the edge sites. The central problem to be addressed in the work is the account of the interparticle interaction. We shall examine the stability of nonlinear BIC in the classical regime and investigate the link between the classical and quantum solutions. It shall be demonstrated that even a classically stable nonlinear BIC undergoes a slow rate decay due to quantum fluctuations. Thus, the antisymmetric BEC of interacting particles is always a metastable state. We shall show that the quantum fluctuations can be accurately described within the pseudoclassical framework by the stochastic force emerging in the nonlinear coupled oscillator model.

II. MASTER EQUATION AND PSEUDOCLASSICAL APPROACH

We consider a linear trimer of three coupled potential wells. The trimer is initially occupied by N_0 bosons which can tunnel between the wells as shown in Fig. 1. The tunneling dynamics is controlled by the Bose-Hubbard Hamiltonian,

$$\widehat{\mathcal{H}} = -\frac{J}{2}\sum_{\ell=1}^{2}(\hat{a}_{\ell+1}^{\dagger}\hat{a}_{\ell} + \text{H.c.}) + \frac{U}{2}\sum_{\ell=1}^{3}\hat{n}_{\ell}(\hat{n}_{\ell}-1), \qquad (1)$$

where $\hat{a}_{\ell}^{\dagger}(\hat{a}_{\ell})$ is the creation (annihilation) operator at the ℓ_{th} site, $\hat{n}_{\ell}$ is the number operator at the ℓ_{th} site, J is the interwell tunneling rate, and U is the interaction constant. By now the BH model has grown into one of the seminal models in physics of cold atoms which scopes quantum phase transitions [32], the effects of Josephson oscillations [33,34], atomic Bloch oscillations [35,36], refill dynamics in the presence of induced losses [14,37], spontaneous breaking of the symmetry [38], and quantized current in the engineered transport channel [7,9,10] to mention a few results relevant to the present paper. Here, following [15], we assume that the central well is attached to a particle sink as shown in Fig. 1. Then the system dynamics is described by the density matrix $\widehat{\mathcal{R}}$ which obeys the master equation,

$$\frac{\partial\widehat{\mathcal{R}}}{\partial t} = -i[\widehat{\mathcal{H}},\widehat{\mathcal{R}}] + \widehat{\mathcal{L}}(\widehat{\mathcal{R}}), \qquad (2)$$

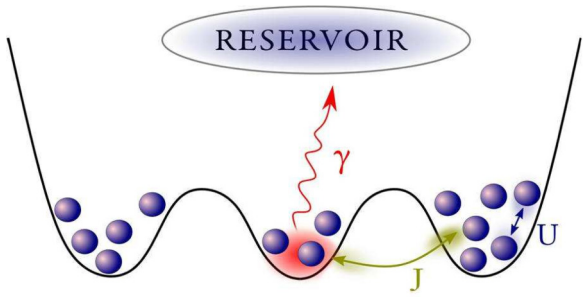

FIG. 1. Sketch of the system.

with the loss operator of a Lindblad form,

$$\widehat{\mathcal{L}}(\widehat{\mathcal{R}}) = -\frac{\gamma}{2}(\hat{a}_2^\dagger \hat{a}_2 \widehat{\mathcal{R}} - 2\hat{a}_2 \widehat{\mathcal{R}} \hat{a}_2^\dagger + \widehat{\mathcal{R}} \hat{a}_2^\dagger \hat{a}_2), \tag{3}$$

where γ is the loss rate.

The pseudoclassical approach is introduced by replacing each operator $\widehat{A}$ by its Weyl symbol which is a function on the phase space [39],

$$\mathrm{symb}[\widehat{A}] = A(a, a^*), \tag{4}$$

with a, a^* being the complex conjugated canonical variables defined as the Weyl symbols of the annihilation and creation operators,

$$\mathrm{symb}[\hat{a}] = a, \ \mathrm{symb}[\hat{a}^\dagger] = a^*, \tag{5}$$

where we omitted the subindex ℓ for simplicity. The Weyl symbols of an operator product of two operators are computed via the Moyal star product of the Weyl symbols of the two operators,

$$A \star B = A \exp\left[\frac{\hbar}{2}\left(\frac{\partial^\leftarrow}{\partial a}\frac{\partial^\rightarrow}{\partial a^*} - \frac{\partial^\leftarrow}{\partial a^*}\frac{\partial^\rightarrow}{\partial a}\right)\right] B. \tag{6}$$

For instance, it is easy to see from Eq. (6) that the Weil symbol of the number operator is

$$\mathrm{symb}[\hat{n}] = a^* \star a = |a|^2 - \tfrac{1}{2}. \tag{7}$$

The figure of merit in the pseudoclassical approach is the Weyl symbol of the density matrix known as the Wigner function,

$$\mathcal{W} = \mathrm{symb}[\widehat{\mathcal{R}}]. \tag{8}$$

Applying Eq. (6) to the master equation, Eq. (2) one finds that the Wigner function obeys the following equation [40,41]:

$$\begin{aligned}\frac{\partial \mathcal{W}}{\partial t} = &-i\sum_{\ell=1}^{3}\left[U\left(1-|\alpha_\ell^2|\right)\left(\alpha_\ell\frac{\partial \mathcal{W}}{\partial \alpha_\ell} - \alpha_\ell^*\frac{\partial \mathcal{W}}{\partial \alpha_\ell^*}\right) - \ldots\right.\\ &\left. - \frac{U}{4}\left(\frac{\partial^3 \alpha_\ell^* \mathcal{W}}{\partial \alpha_\ell \partial \alpha_\ell^{*2}} - \frac{\partial^3 \alpha_\ell \mathcal{W}}{\partial \alpha_\ell^2 \partial \alpha_\ell^*}\right)\right] - i\frac{J}{2}\sum_{\ell=1}^{2}\left(\alpha_{\ell+1}\frac{\partial \mathcal{W}}{\partial \alpha_\ell}\right.\\ &\left. + \alpha_\ell\frac{\partial \mathcal{W}}{\partial \alpha_{\ell+1}} - \alpha_{\ell+1}^*\frac{\partial \mathcal{W}}{\partial \alpha_\ell^*} - \alpha_\ell^*\frac{\partial \mathcal{W}}{\partial \alpha_{\ell+1}^*}\right)\\ &+ \frac{\gamma}{2}\left(\alpha_2\frac{\partial \mathcal{W}}{\partial \alpha_2} + 2\mathcal{W} + \alpha_2^*\frac{\partial \mathcal{W}}{\partial \alpha_2^*}\right) + \frac{\gamma}{2}\frac{\partial^2 \mathcal{W}}{\partial \alpha_2 \partial \alpha_2^*}.\end{aligned} \tag{9}$$

The above equation contains third-order derivatives which do not allow one to interpret it as a Fokker-Plank equation with a positive definite or positive semidefinite diffusion matrix [40].

The pseudoclassical limit of Eq. (9) is obtained by setting $N_0 \to \infty$ while keeping $g = UN_0 = \mathrm{Const}$. In what follows the quantity g will be referred to as the macroscopic interaction constant. Let us apply the following substitution:

$$\alpha_\ell = \sqrt{N_0}a_\ell, \ \ \alpha_\ell^* = \sqrt{N_0}a_\ell^*. \tag{10}$$

Then Eq. (9) transforms to

$$\begin{aligned}\frac{\partial \mathcal{W}}{\partial t} = &-i\sum_{\ell=1}^{3}\left[g\left(\frac{1}{N_0} - |a_\ell^2|\right)\left(a_\ell\frac{\partial \mathcal{W}}{\partial a_\ell} - a_\ell^*\frac{\partial \mathcal{W}}{\partial a_\ell^*}\right)\right] - i\frac{J}{2}\sum_{\ell=1}^{2}\\ &\times\left(a_{\ell+1}\frac{\partial \mathcal{W}}{\partial a_\ell} + a_\ell\frac{\partial \mathcal{W}}{\partial a_{\ell+1}} - a_{\ell+1}^*\frac{\partial \mathcal{W}}{\partial a_\ell^*} - a_\ell^*\frac{\partial \mathcal{W}}{\partial a_{\ell+1}^*}\right)\\ &+ \frac{\gamma}{2}\left(a_2\frac{\partial \mathcal{W}}{\partial a_2} + 2\mathcal{W} + a_2^*\frac{\partial \mathcal{W}}{\partial a_2^*}\right) + \frac{\gamma}{2N_0}\frac{\partial^2 \mathcal{W}}{\partial a_2 \partial a_2^*}\\ &+ O\left(N_0^{-2}\right).\end{aligned} \tag{11}$$

Neglecting the $O(N_0^{-2})$ term we arrive at a true Fokker-Plank equation where the first term in the third line can be viewed as dissipation while the second term in the same line is diffusion [27,28].

The dynamics under the Fokker-Planck equation, Eq. (11) can be unravelled into a set of dissipative Langevin equations,

$$\begin{aligned} ida_1 &= \left(-\frac{J}{2}a_2 + g|a_1|^2 a_1\right)dt,\\ ida_2 &= \left[-\frac{J}{2}\left(a_1 + a_3\right) + g|a_2|^2 a_2 - i\frac{\gamma}{2}a_2\right]dt + \sqrt{\frac{\gamma}{2N_0}}d\xi,\\ ida_3 &= \left(-\frac{J}{2}a_2 + g|a_3|^2 a_3\right)dt,\end{aligned} \tag{12}$$

where $d\xi$ is the complex white noise,

$$\overline{d\xi} = 0, \ \overline{d\xi^* d\xi} = dt, \ \overline{d\xi d\xi} = 0. \tag{13}$$

Notice that compared to Eq. (9) in Eq. (12) we omitted the "self-energy" term proportional to g/N_0. This can be done as the oscillating factor $\exp(-igt/N_0)$ can be absorbed into the noise Eq. (13) without changing its correlation properties.

Let us assume for a moment that there is no noise term in Eq. (12). Then Eq. (12) has an antisymmetric solution decoupled from the lossy site,

$$\boldsymbol{a}_{\mathrm{BIC}}(t) = e^{-igIt}\begin{pmatrix}\sqrt{I}\\ 0\\ -\sqrt{I}\end{pmatrix}, \tag{14}$$

where the intensity I can be linked to the mean population of the edge sites $\overline{n}_{1,3} = IN_0 + 1/2$. By examination of Eq. (12) one immediately identifies the three factors affecting the decay dynamics of this state.

(i) The stability of the BIC. If solution (14) is unstable, it can be destroyed by small perturbations.

(ii) The initial condition for solving Eq. (12). In more detail, we expect that the decay rate is dependent on how close the initial condition is to the symmetry-protected BIC, Eq. (14). Moreover, in establishing quantum to classical correspondence one cannot deal with a single trajectory but with the ensemble of trajectories whose initial conditions are

determined by the initial many-body quantum state of the system [24].

(iii) The noise term in Eq. (12) inversely proportional to $\sqrt{N_0}$. The noise can perturb even an intrinsically stable state driving it out of equilibrium. Notice that even though the reservoir does not supply particles into the system a stochastic driving force is still present in Eq. (12). Physically, this intrinsic noise is nothing but the quantum fluctuations arising from the noncommutativity of creation and annihilation operators. The noise term is important for the correct application of the pseudoclassical approach. For example, in the paradigm problem of the decaying quantum oscillator it ensures that the oscillator does not decay below its ground energy.

In the next section we discuss each of these factors in more detail.

III. DECAY OF THE ANTISYMMETRIC STATE

A. Stability analysis

First we analyze the stability of the solution $\boldsymbol{a}_{\rm BIC}(t)$ for $g \neq 0$. Using the standard stability analysis [42] the stability of this solution can be examined by analyzing the matrix,

$$\widehat{M} = \begin{pmatrix} gI & -J/2 & 0 & gI & 0 & 0 \\ -J/2 & -i\gamma/2 - gI & -J/2 & 0 & 0 & 0 \\ 0 & -J/2 & gI & 0 & 0 & gI \\ -gI & 0 & 0 & gI & J/2 & 0 \\ 0 & 0 & 0 & J/2 & -i\gamma/2 + gI & J/2 \\ 0 & 0 & -gI & 0 & J/2 & gI \end{pmatrix}. \tag{15}$$

If the imaginary part of all eigenvalues of $\widehat{M}$ is nonpositive, the BIC solution is stable. Figure 2(a) shows the imaginary parts of the eigenvalues as the function of gI for $J = 1$ and $\gamma = 0.4$. It is seen that in this case the stability threshold corresponds to $|gI| = 0.2$ and is independent on the sign of the interaction constant. Further on we shall only consider repulsive interactions. Above the threshold any tiny imbalance in the population of the edge sites will lead to excitation of the symmetric modes and the BIC loses its intensity. This process is exponential in time resulting in a rapid drop of intensity at the initial stage. However, once the stability threshold is crossed the solution $\boldsymbol{a}_{\rm BIC}(t)$ stabilizes at a certain value of intensity $I_{\rm st}$,

$$I_{\rm st} = I_{\rm st}(\gamma, g). \tag{16}$$

In what follows we shall refer to Eq. (16) as the stabilization level. We mention that, as expected, the stabilization level is approximately inversely proportional to g yet it is always smaller than the stability threshold deduced from Eq. (15). The described scenario is exemplified by thin solid lines in Figs. 2(d) and 2(e) where, to provoke the symmetry breaking, we introduced a tiny population imbalance $\sim 10^{-3}$ in the initial BIC state. The exponential decrease of intensity for g above the stability threshold and the effect of stabilization is clearly seen in the figure.

B. Quantum ensemble

Before simulating the decay of truly quantum states we have to introduce an ensemble of classical initial conditions corresponding to a quantum state loaded into the system. This can be done by using the Husimi $\mathcal{Q}$ function,

$$\mathcal{Q}(\boldsymbol{\alpha}) = \frac{1}{\pi^3}\langle\boldsymbol{\alpha}|\widehat{\mathcal{R}}|\boldsymbol{\alpha}\rangle, \tag{17}$$

where $|\boldsymbol{\alpha}\rangle$ is the Glauber coherent state,

$$|\boldsymbol{\alpha}\rangle = e^{-\frac{|\alpha_1|^2+|\alpha_2|^2+|\alpha_3|^2}{2}} e^{\alpha_1\hat{a}_1^\dagger+\alpha_2\hat{a}_2^\dagger+\alpha_3\hat{a}_3^\dagger}|{\rm vac}\rangle, \tag{18}$$

with $\boldsymbol{\alpha} = \{\alpha_1, \alpha_2, \alpha_3\}$. At first, for the initial state we choose an antisymmetric N-particle BEC. However, for future convenience below we present a single formula for both symmetric $|\Psi^{(+)}_{\rm BEC}\rangle$ and antisymmetric $|\Psi^{(-)}_{\rm BEC}\rangle$ condensates,

$$|\Psi^{(\pm)}_{\rm BEC}\rangle = \frac{1}{\sqrt{2^N N!}}(\hat{a}_1^\dagger \pm \hat{a}_3^\dagger)^N|{\rm vac}\rangle. \tag{19}$$

After applying the Husimi transformation Eq. (17) one finds

$$\mathcal{Q}^{(\pm)}_{\rm BEC}(\boldsymbol{\alpha}) = \frac{|\alpha_1 \pm \alpha_3|^{2N}}{\pi^3 2^N (N!)} e^{-|\alpha_1|^2-|\alpha_2|^2-|\alpha_3|^2}. \tag{20}$$

It is worth mentioning that in [24] the quantum ensemble was generated by using the SU($\boldsymbol{L}$) coherent states which specifically refer to the problems with conserved number of particles. In case, since the number of particles is not conserved, the application of the Glauber coherent states is more appropriate. By applying the acception-rejection method [24] we generate the ensembles of the initial conditions according to the distribution function (20) for $N_0 = 20$ and $N_0 = 100$; see Figs. 2(b) and 2(c). The width of the depicted distribution scales as $\sqrt{N_0}$ for the amplitudes and $1/\sqrt{N_0}$ for the relative phases. Now, having the quantum ensemble at hand we can simulate the system dynamics. The result is depicted by the thick dashed lines in Figs. 2(d) and 2(e). Notice that according to Eqs. (10) and (14) the initial intensity is always $I = 1/2$, thus, the stability threshold $gI = 0.20$ in Fig. 2(a) corresponds to $g = 0.40$ in the initial time. Remarkably, in the unstable cases ($g > 0.4$) we get the same fraction of bosons which is left in the system as it is predicted by the pure classical stability analysis given in the previous subsection. In the stable case $g = 0.4$, however, we observe essential deviations. These can be understood by noticing that every initial condition $\mathbf{a}(t = 0)$ from the quantum ensemble is a superposition of the system linear eigenmodes,

$$\boldsymbol{b}_1 = \begin{pmatrix} \frac{1}{\sqrt{2}} \\ 0 \\ \frac{-1}{\sqrt{2}} \end{pmatrix}, \ \boldsymbol{b}_2 = \begin{pmatrix} \frac{1}{2} \\ \frac{1}{\sqrt{2}} \\ \frac{1}{2} \end{pmatrix}, \ \boldsymbol{b}_3 = \begin{pmatrix} \frac{1}{2} \\ \frac{-1}{\sqrt{2}} \\ \frac{1}{2} \end{pmatrix}, \tag{21}$$

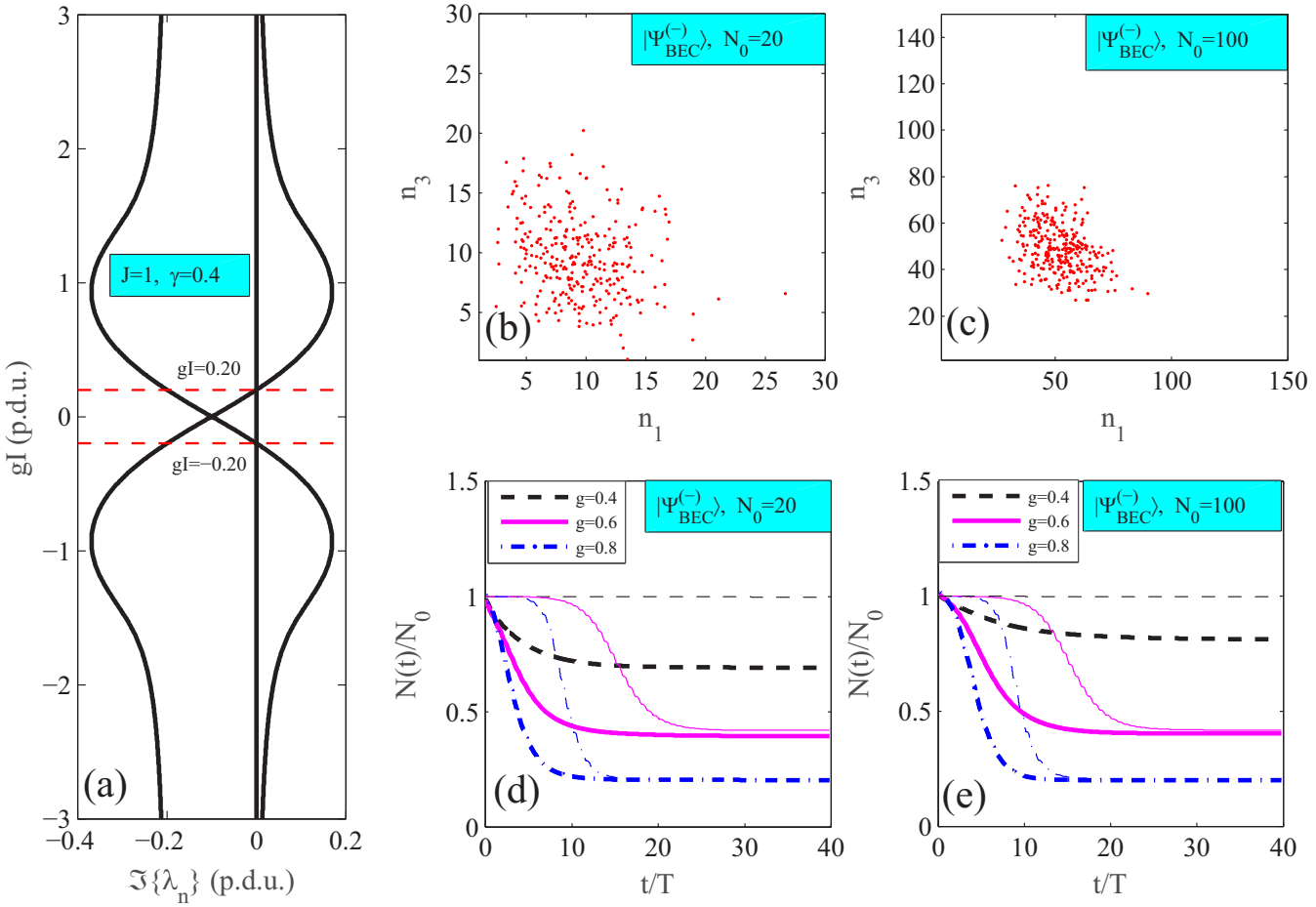

FIG. 2. (a) Thick solid lines show the imaginary parts $\mathrm{Im}\{\lambda_n\}$ of the eigenvalues of matrix (15) for $J = 1$, $\gamma = 0.4$. Thin dashed lines show the stability threshold. (b) and (c) Initial conditions for the antisymmetric BEC in the space of populations of the first, n_1, and the third, n_3, sites for (b) $N_0 = 20$ and (c) $N_0 = 100$. (d) and (e) Decay dynamics of the antisymmetric state with (d) $N_0 = 20$ and (e) $N_0 = 100$. Thick lines show the total number of particles against time for antisymmetric BEC initial conditions shown in subplot [(d) and (c)]. Thin lines show the decay of the classical BIC state.

where the first eigenmode obviously corresponds to the symmetry-protected BIC while the other two modes are coupled to the reservoir and decay within the characteristic time $2\pi/\gamma$. Thus, the solid and dashed lines in Figs. 2(d) and 2(e) may coincide only in the limit $N_0 \to \infty$ where the quantum ensemble shrinks to the single point.

C. The role of the noise

Now let us return to the Langevin dynamics governed by Eq. (12) where one could expect that even a stable antisymmetric BIC state Eq. (14) is subject to decay. To test this conjecture we solve numerically both the Langeven equation and the exact master equation, Eq. (2). The results are shown in Fig. 3. In Fig. 3(a) we depict the exact quantum solution for the total population. One can see that unlike the classical solutions in Fig. 2 the population now continues to decay even after crossing the stabilization level. This decay is still exponential, however, with much smaller rate. In Fig. 3(b) we compare the population dynamics for the first and the second sites obtained by the pseudoclassical and quantum approaches. One can see that the two results are in good agreement. This supports our conjecture that the noise destroys the classical symmetry-protected BIC.

To look at the decay dynamics in more detail we compute the single-particle density matrix $\hat{\rho}$, whose matrix elements are defined as

$$\rho_{\ell,\ell'} = \mathrm{Tr}(\hat{a}^\dagger_\ell \hat{a}_{\ell'} \widehat{\mathcal{R}}). \tag{22}$$

In the pseudoclassical framework this matrix corresponds to the correlation functions,

$$\rho_{\ell,\ell'} = \langle a^*_\ell a_{\ell'} \rangle - \tfrac{1}{2}\delta_{\ell,\ell'}, \tag{23}$$

where the pointy brackets designate the ensemble average over Langevin trajectories. The single-particle density matrix allows us to test whether the quantum state remains a BEC during the decay [43]. Namely, if all but one eigenvalues are zero the system is a condensate state. Another related quantity is the correlation function [15],

$$C(t) = \frac{\rho_{1,3}}{\sqrt{\rho_{1,1}\rho_{3,3}}} = \frac{\langle a^*_1 a_3 \rangle}{\sqrt{\langle |a_1|^2 \rangle \langle |a_3|^2 \rangle}}. \tag{24}$$

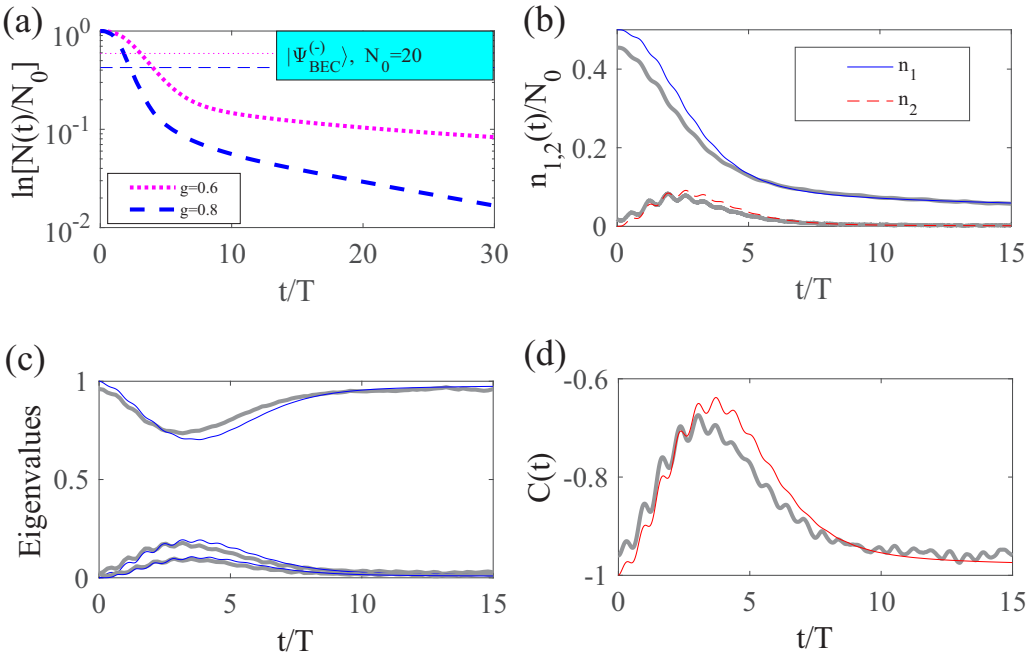

FIG. 3. Decay of the antisymmetric condensate for $N_0 = 20$. (a) Thick lines are logarithmic plots of the total population against time obtained by solving the master equation Eq. (2). Thin lines show the stabilization levels from Fig. 2(d). (b) Populations of the first and the second sites against time. Here and in (c) and (d) thin lines are quantum simulations while thick gray lines are the results of the pseudoclassical approach, $g = 0.8$. (c) Normalized eigenvalues of the single-particle density matrix Eq. (22), $g = 0.8$. (c) Correlation function Eq. (24), $g = 0.8$.

If $C(t) = -1$ the system is an antisymmetric condensate and if $C(t) = 1$, then the condensate is symmetric. In Fig. 3(c) we show the normalized eigenvalues of $\hat{\rho}$, while in Fig. 3(d) we plotted the correlation functions, Eq. (24). Both subplots are consistent with the decay dynamics described above: First, the system rapidly departs from antisymmetric BEC. Then, after the stabilization level is crossed the system recoheres into antisymmetric BEC

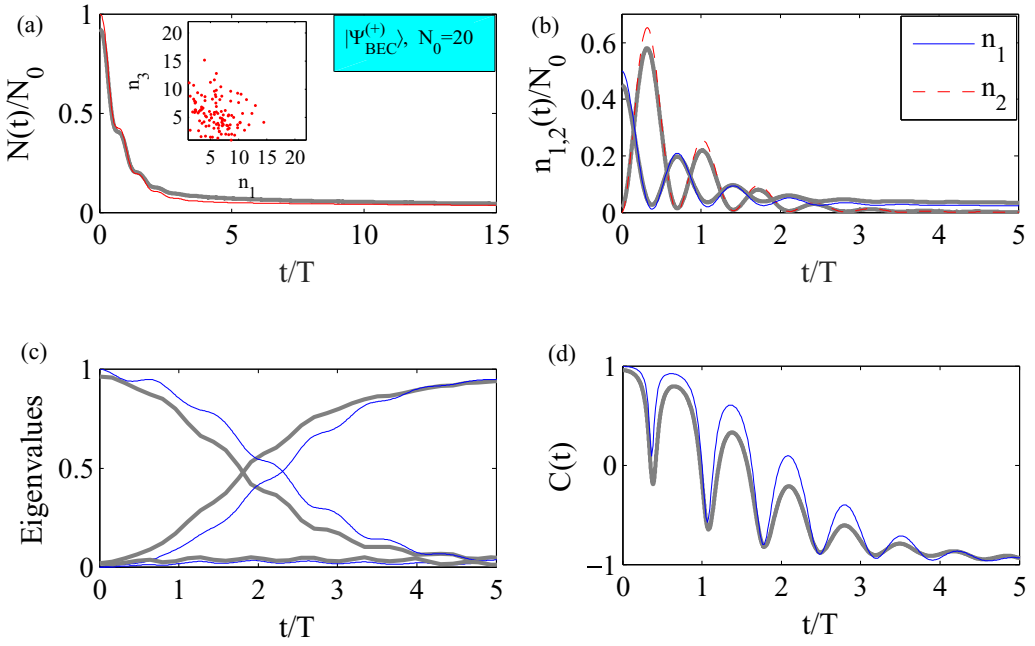

FIG. 4. Decay of symmetric condensate for $g = 0.8$ and $N_0 = 20$; thin lines—quantum simulations, thick gray lines—pseudoclassical approach. (a) The full population against time as obtained by solving the master equation Eq. (2). The inset shows the ensemble of initial conditions. (b) Populations of the first and the second wells against time. (c) Normalized eigenvalues of the single-particle density matrix Eq. (22). (d) Correlation function Eq. (24).

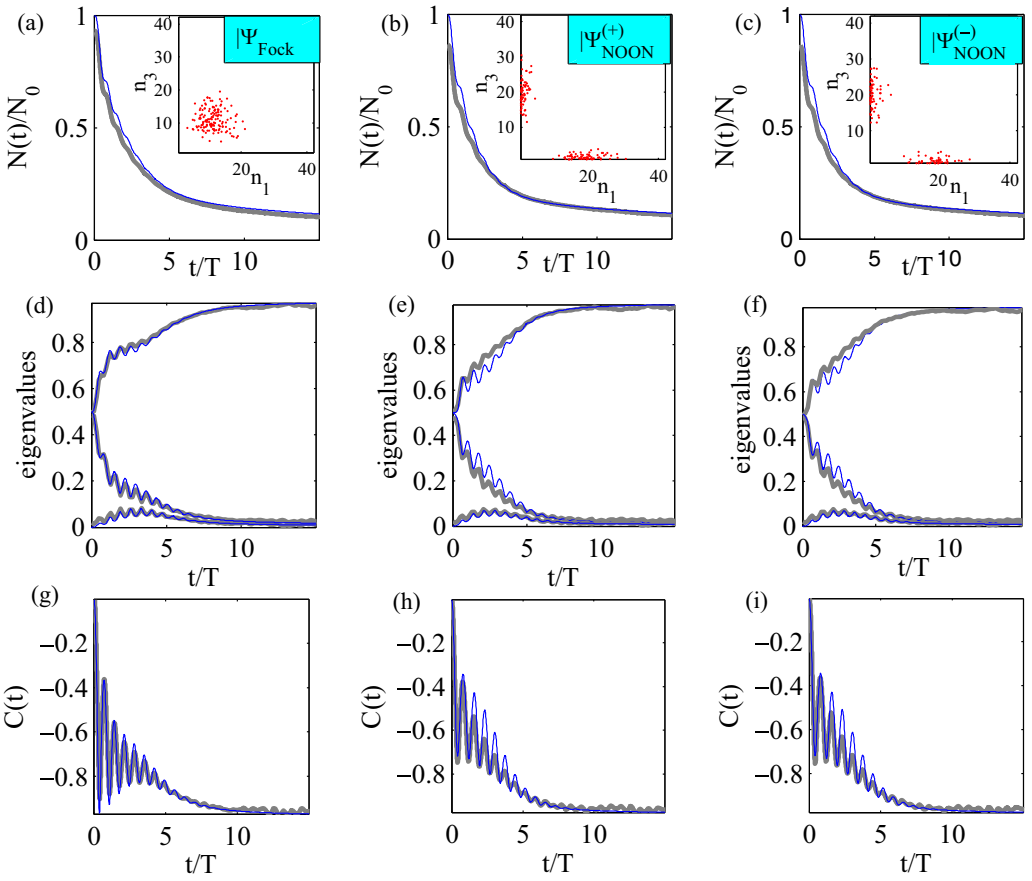

FIG. 5. Decay of fragmented condensates, $N_0 = 20$, $T = 2\pi$ (p.d.u.); thick gray lines show the result by the pseudoclassical approach, thin blue lines show the solutions of the master equations. (a)–(c) Dynamics of the full population. The insets show the ensembles of initial conditions. (d)–(f) Normalized eigenvalues of the single-particle density matrix for (d) Fock state, (e) symmetric NOON state, and (f) antisymmetric NOON state. (g)–(i) Correlation function, Eq. (24) for (g) Fock state, (h) symmetric NOON state, and (i) antisymmetric NOON state.

again and slowly decays as the metastable antisymmetric solution.

D. Symmetric BEC

To see the full picture in this section we also present results on the decay of the symmetric BEC state, Eq. (19). One can see from Fig. 4 that in the course of time the symmetric BEC state rapidly drops intensity and decoheres into a fragmented condensate with two nonzero eigenvalues of the single-particle density matrix. Eventually, only a tiny fraction of the initial population survives after the system transits into a pure antisymmetric BEC well below the stability threshold. Again we see a good coincidence between the quantum and pseudoclassical results.

IV. DECAY OF FRAGMENTED CONDENSATES

Next we examine the decay dynamics of fragmented condensate states. The fragmented condensate states are defined as those having more than one nonzero eigenvalue of the single-particle density matrix [43]. The most obvious example of a fragmented condensate is a Fock state,

$$|\Psi_{\rm Fock}\rangle = \frac{1}{(N/2)!}(\hat{a}_1^\dagger \hat{a}_3^\dagger)^{(N/2)}|{\rm vac}\rangle, \tag{25}$$

where $N/2$ particles occupy the first site and the rest $N/2$ particles are in the third site. Directly applying Eq. (17) one finds

$$\mathcal{Q}_{\rm Fock}(\boldsymbol{\alpha}) = \frac{|\alpha_1|^N|\alpha_3|^N}{\pi^3[(N/2)!]^2} e^{-|\alpha_1|^2-|\alpha_2|^2-|\alpha_3|^2}. \tag{26}$$

Another, less trivial, example is the (anti-)symmetric NOON state which is a Schrödinger cat state of N bosons in two wells,

$$|\Psi^{(\pm)}_{\rm NOON}\rangle = \frac{1}{\sqrt{2(N!)}}[(\hat{a}_1^\dagger)^N \pm (\hat{a}_3^\dagger)^N]|{\rm vac}\rangle. \tag{27}$$

This state has the following $\mathcal{Q}$ function,

$$\mathcal{Q}^{(\pm)}_{\rm NOON}(\boldsymbol{\alpha}) = e^{-|\alpha_1|^2-|\alpha_2|^2-|\alpha_3|^2} \times \frac{|\alpha_1|^{2N} + |\alpha_3|^{2N} \pm (\alpha_1\alpha_3^*)^N \pm (\alpha_1^*\alpha_3)^N}{\pi^3 2(N!)}. \tag{28}$$

In Fig. 5 we show the simulation results by both pure quantum and pseudoclassical approaches. One can see that despite the profound difference between the Fock state and the (anti-)symmetric NOON states clearly seen in insets in Fig. 5(a)–5(c), the decay dynamics is essentially identical. In all cases we see a rapid decay of a fragmented state below the stability threshold after which the system recoheres to the antisymmetric BEC having lost the major part of the initial population. As before we see a good accuracy of the pseudoclassical approach.

V. SUMMARY AND CONCLUSIONS

We have examined the decay dynamics of quantum states with a definite number of bosons in the three-well open Bose-Hubbard model. It is demonstrated that the stability of the quantum state can be predicted from the classical perspective. The decay scenarios are drastically different depending on whether the solution is stable in the pseudoclassical limit. In particular, it is shown that in the pseudoclassical regime the antisymmetric BEC state is mapped to a symmetry-protected bound state in the continuum (BIC). The BIC is only stable below a certain intensity threshold. Above the classical stability threshold the antisymmetric BEC rapidly decays and decoheres due to interparticle interactions. Once the population has dropped below the threshold, however, the system recoheres to the antisymmetric BEC which decays at a much slower rate due to the quantum fluctuations. It is demonstrated that the quantum fluctuations can be accurately described in the pseudoclassical framework by introducing a stochastic force with amplitude inversely proportional to the square root of the initial number of particles.

The pseudoclassical approach has been applied to several types of initial states with initial population only at the edge sites. Besides the antisymmetric BEC we have studied the decay of symmetric BEC, Fock, (anti-) symmetric NOON states. In all cases the initial bosonic cloud rapidly looses population to the reservoir and the decay can only slow down well below the classical stability threshold when the system recoheres to the metastable antisymmetric BEC. In all cases we observed a good coincidence between the numerical data obtained by the pseudoclassical approach and exact quantum simulations.

Recently, we have seen a surge of interest in decay dynamics of two-photon states [44–47]. We believe that the approach presented here provides the key to understanding the decay dynamics in the other solvable limit, namely, pseudoclassical regime. Finally, we would like to outline the future work ensuing from the present paper. It remains a question whether the asymptotic law of below threshold decay can be derived from the Langevin equations, Eq. (12), or the corresponding Fokker-Plank equation. We speculate that this problem may pose an interesting topic for future research.

ACKNOWLEDGMENTS

This work has been supported by Russian Science Foundation through Grant No. N19-12-00167. We appreciate discussions with A. F. Sadreev and E. N. Bulgakov. We are also grateful to G. P. Fedorov for his critical reading of the manuscript.

[1] S. Diehl, A. Micheli, A. Kantian, B. Kraus, H. P. Büchler, and P. Zoller, Nat. Phys. **4**, 878 (2008).
[2] Y. Lin, J. P. Gaebler, F. Reiter, T. R. Tan, R. Bowler, A. S. Sørensen, D. Leibfried, and D. J. Wineland, Nature (London) **504**, 415 (2013).
[3] F. Verstraete, M. M. Wolf, and J. I. Cirac, Nat. Phys. **5**, 633 (2009).
[4] D. Witthaut, F. Trimborn, and S. Wimberger, Phys. Rev. Lett. **101**, 200402 (2008).
[5] T. Prosen and B. Žunkovič, New J. Phys. **12**, 025016 (2010).
[6] P. Barmettler and C. Kollath, Phys. Rev. A **84**, 041606(R) (2011).
[7] J.-P. Brantut, J. Meineke, D. Stadler, S. Krinner, and T. Esslinger, Science **337**, 1069 (2012).
[8] G. Barontini, R. Labouvie, F. Stubenrauch, A. Vogler, V. Guarrera, and H. Ott, Phys. Rev. Lett. **110**, 035302 (2013).
[9] S. Krinner, D. Stadler, D. Husmann, J.-P. Brantut, and T. Esslinger, Nature (London) **517**, 64 (2015).
[10] M. Lebrat, P. Grišins, D. Husmann, S. Häusler, L. Corman, T. Giamarchi, J.-P. Brantut, and T. Esslinger, Phys. Rev. X **8**, 011053 (2018).
[11] R. A. Pepino, J. Cooper, D. Meiser, D. Z. Anderson, and M. J. Holland, Phys. Rev. A **82**, 013640 (2010).
[12] A. Ivanov, G. Kordas, A. Komnik, and S. Wimberger, Eur. Phys. J. B **86**, 345 (2013).
[13] A. R. Kolovsky, Z. Denis, and S. Wimberger, Phys. Rev. A **98**, 043623 (2018).
[14] R. Labouvie, B. Santra, S. Heun, and H. Ott, Phys. Rev. Lett. **116**, 235302 (2016).
[15] G. Kordas, D. Witthaut, and S. Wimberger, Ann. Phys. **527**, 619 (2015).
[16] K. Nemoto, C. A. Holmes, G. J. Milburn, and W. J. Munro, Phys. Rev. A **63**, 013604 (2000).
[17] R. Franzosi and V. Penna, Phys. Rev. A **65**, 013601 (2001).
[18] R. Franzosi and V. Penna, Phys. Rev. E **67**, 046227 (2003).
[19] A. A. Bychek, P. S. Muraev, D. N. Maksimov, and A. R. Kolovsky, in *Fifth International Conference on Quantum Technologies (ICQT-2019)*, edited by A. Fedorov and A. Rubtsov, AIP Conf. Proc. No. 2241 (AIP, New York, 2020), p. 02007
[20] K. W. Mahmud, H. Perry, and W. P. Reinhardt, Phys. Rev. A **71**, 023615 (2005).
[21] S. Mossmann and C. Jung, Phys. Rev. A **74**, 033601 (2006).
[22] E. M. Graefe and H. J. Korsch, Phys. Rev. A **76**, 032116 (2007).
[23] F. Trimborn, D. Witthaut, and H. J. Korsch, Phys. Rev. A **77**, 043631 (2008).

[24] A. R. Kolovsky, H.-J. Korsch, and E.-M. Graefe, Phys. Rev. A **80**, 023617 (2009).
[25] T. Zibold, E. Nicklas, C. Gross, and M. K. Oberthaler, Phys. Rev. Lett. **105**, 204101 (2010).
[26] A. A. Bychek, D. N. Maksimov, and A. R. Kolovsky, Phys. Rev. A **97**, 063624 (2018).
[27] A. A. Bychek, P. S. Muraev, and A. R. Kolovsky, Phys. Rev. A **100**, 013610 (2019).
[28] A. A. Bychek, P. S. Muraev, D. N. Maksimov, and A. R. Kolovsky, Phys. Rev. E **101**, 012208 (2020).
[29] C. W. Hsu, B. Zhen, A. D. Stone, J. D. Joannopoulos, and M. Soljačić, Nat. Rev. Mater. **1**, 16048 (2016).
[30] E. Bulgakov, K. Pichugin, and A. Sadreev, J. Phys.: Condens. Matter **23**, 065304 (2011).
[31] E. Bulgakov, K. Pichugin, and A. Sadreev, Phys. Rev. B **83**, 045109 (2011).
[32] M. Greiner, O. Mandel, T. Esslinger, T. W. Hänsch, and I. Bloch, Nature (London) **415**, 39 (2002).
[33] R. Gati and M. K. Oberthaler, J. Phys. B: At., Mol. Opt. Phys. **40**, R61 (2007).
[34] J. Estève, C. Gross, A. Weller, S. Giovanazzi, and M. K. Oberthaler, Nature (London) **455**, 1216 (2008).
[35] F. Meinert, M. J. Mark, E. Kirilov, K. Lauber, P. Weinmann, M. Gröbner, and H.-C. Nägerl, Phys. Rev. Lett. **112**, 193003 (2014).
[36] C. J. Fujiwara, K. Singh, Z. A. Geiger, R. Senaratne, S. V. Rajagopal, M. Lipatov, and D. M. Weld, Phys. Rev. Lett. **122**, 010402 (2019).
[37] R. Labouvie, B. Santra, S. Heun, S. Wimberger, and H. Ott, Phys. Rev. Lett. **115**, 050601 (2015).
[38] A. Trenkwalder, G. Spagnolli, G. Semeghini, S. Coop, M. Landini, P. Castilho, L. Pezze, G. Modugno, M. Inguscio, A. Smerzi *et al.*, Nat. Phys. **12**, 826 (2016).
[39] S. W. McDonald, Phys. Rep. **158**, 337 (1988).
[40] K. Vogel and H. Risken, Phys. Rev. A **38**, 2409 (1988).
[41] D. Bortman and A. Ron, Phys. Rev. A **52**, 3316 (1995).
[42] A. J. Lichtenberg and M. A. Lieberman, *Regular and Chaotic Dynamics* (Springer Science & Business Media, Berlin/Heidelberg, 2013) Vol. 38.
[43] E. J. Mueller, T.-L. Ho, M. Ueda, and G. Baym, Phys. Rev. A **74**, 033612 (2006).
[44] A. Crespi, L. Sansoni, G. Della Valle, A. Ciamei, R. Ramponi, F. Sciarrino, P. Mataloni, S. Longhi, and R. Osellame, Phys. Rev. Lett. **114**, 090201 (2015).
[45] H. L. Chen, G. Wang, and R. K. Lee, Opt. Express **26**, 33205 (2018).
[46] Y.-X. Zhang, C. Yu, and K. Mølmer, Phys. Rev. Res. **2**, 013173 (2020).
[47] A. N. Poddubny, Phys. Rev. A **101**, 043845 (2020).